ACS APPLIED MATERIALS & INTERFACES

Research Article

www.acsami.org

Synthesis of Nanostructured Silver/Silver Halides on Titanate Surfaces and Their Visible-Light Photocatalytic Performance

Yuxin Tang,[†] Zhelong Jiang,[†] Jiyang Deng,[†] Dangguo Gong,[†] Yuekun Lai,[†] Han Teng Tay,[†] Ivor Tan Kian Joo,[‡] Teck Hua Lau,[†] Zhili Dong,*[,†] and Zhong Chen*[,†]

[†]School of Materials Science and Engineering, Nanyang Technological University, 50 Nanyang Avenue, 639798, Singapore

[‡]Faculty of Civil and Environmental Engineering, Universiti Tun Hussein Onn Malaysia, 86400 Johor, Malaysia

Supporting Information

ABSTRACT: Dense and uniform silver halides AgX (X = Cl, Br, I) nanoparticles were successfully fabricated on layered titanate nanowired honeycomb (TNHC) thin films. The growth of AgX nanocrystals was carried out through two steps. Firstly, ion-exchange was employed to incorporate Ag^+ ions into the interlayer of the titanate nanowires. Secondly, hydrogen halide (HX) solution was rapidly injected onto the ion-exchanged silver TNHC surface to generate nanosized AgX particles on TNHC films. The effect of the reaction time, solution pH, and concentration of halide anions on the morphology of the AgX photocatalysts has been studied. Followed by light-irradiation, the optimized Ag/AgX thin films exhibited excellent degradation performance under visible light because of localized surface plasmon resonance effect.

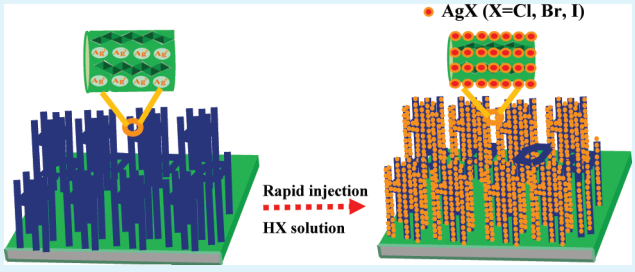

KEYWORDS: *photocatalyst, titanate material, silver halide, visible light activity, surface plasmon resonance, ion-exchange*

1. INTRODUCTION

Models of photosynthesis mimetic systems, or artificial photosynthesis systems, including photoelectrochemical water splitting, photocatalysis and photovoltaic cells, have attracted significant amount of attention because of the abundance of solar resource available, and minimum carbon footprint generated by these systems.[1−3] Semiconductor photocatalysts, such as TiO_2, ZnO, Fe_2O_3, WO_3, etc., have been shown to be able to effectively photocatalyze many chemical reactions. Among them, TiO_2 is one of the most promising candidates. As TiO_2 only absorbs light in the ultraviolet region of the solar light spectrum,[3] various strategies have been explored to broaden its photocatalytic response to visible light, including elemental substitution technique, dye or nanocrystal sensitized heterojunction approach, and composite metal oxides method. However, absorption toward visible light with enhanced photocatalytic activity is still the bottleneck for these photocatalysts to meet the requirements of practical applications.[4]

Recently, novel plasmonic photocatalysts has emerged as an alternative and promising route for developing highly efficient visible-light photocatalyst. Nanoparticles (NPs) of noble metals which exhibit surface plasmon resonance (SPR) effect arising from the collective oscillation of the conduction electrons upon interaction with electromagnetic radiation, can dramatically amplify the absorption of visible light, resulting in the enhanced photocatalytic activity.[5−10] Recent intensive studies have indicated that the silver halides and silver on silver halides structures possess excellent photocatalytic activity and high stability under solar irradiation.[6,11−20] For examples, Hu et al.[12] demonstrated that the introduction of Ag/AgBr in TiO_2 can enhance the photocatalytic activity for the destruction of azodyes and bacteria under visible light. Apatite-coated Ag/AgBr/TiO_2 visible-light photocatalyst prepared by Elahifard et al.[21] also showed a significantly high photocatalytic activity for destruction of bacteria. Huang's group[7,9,22] recently developed a series of Ag@AgX (X = Cl, Br, I) for organic molecule degradation under visible light, and they found that their degradation rate was several times higher than the nitrogen-doped TiO_2. Using a rational in situ ion exchange reaction method, they also prepared a new Ag/AgBr/BiOBr hybrid that showed enhanced photocatalytic activity.[23] Sun et al. have synthesized sunlight-driven Ag/AgCl monodispersed NPs in ethylene glycol with the assistance of polyvinylpyrrolidone (PVP) surfactant.[16] Also, the uniformly distributed Ag or Au NPs on AgCl nanowires were prepared via in-situ oxidation of Ag nanowires in Fe^{3+} solution with PVP.[14,24] More recently, a new Ag@AgX/graphene nanocomposites were designed via water/oil approach[4] and deposition−precipitation method.[25] Zhu et al.[26] demonstrated the photocatalytic activity of Ag/AgCl/graphene nanostructures under the sunlight condition. These plasmonic photocatalysts showed wide visible light absorption range as well as improved degradation performance. All those studies have demonstrated the feasibility of silver halides in nanoparticle forms, but there is limited work on the

Received: October 31, 2011
Accepted: December 19, 2011
Published: December 19, 2011

Scheme 1. Schematic Illustration of the In situ Formation Process for AgX/TNHC Hybrid Nanowires[a]

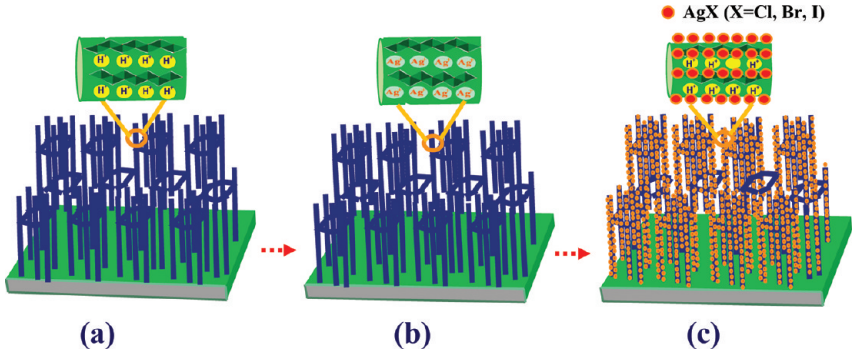

[a](a) H-TNHC is obtained after ion-exchanging Na-TNHC in HNO_3 solution; (b) Ag-TNHC is obtained after ion-exchanging H-TNHC in $AgNO_3$ solution; (c) AgX/TNHC is obtained after reacting Ag-TNHC with the HX (X = Cl, Br, I) solution by rapid injection method. The inset images in (a) and (b) show that the H^+ and Ag^+ ions are distributed uniformly within the nanoscale interlayers of TiO_6 octahedral sheets respectively. The inset image in (c) demonstrates the AgX (X = Cl, Br, I) nanoparticles are formed in situ on the surface of TNHC structures.

synthesis of nano-sized plasmonic photocatalysts on immobilized surfaces, which enjoys a great advantage for handling and reuse in practical photocatalytic applications. Yu et al.[15] demonstrated that Ag/AgCl NPs could be immobilized on TiO_2 nanotube via an impregnating-precipitation−photoreduction method and the nanocomposite photocatalyst exhibited a high visible-light photocatalytic activity. The multitime impregnating−precipitation can introduce more AgCl NPs on nanotube but it is difficult to achieve a dense distribution. In our previous work, a gas phase reaction method was applied to synthesize large-scale AgCl nanocrystal on titanate materials.[27] However, this method still poses some limitations; for example, it is difficult to prepare uniformly distributed AgBr or AgI crystals because of the limited evaporation of gases from even high concentration HBr or HI solutions. Therefore, there is a need to develop a general approach with a facile and inexpensive scheme without surfactant to achieve controllable morphologies with highly and uniformly distributed AgX (AgCl, AgBr, AgI) NPs on a thin film surface. Herein, we present the formation of Ag/AgX NPs on a large-scaled hydrogen titanate nanowired honeycomb film by a rapid injection method. By using the unique ion-exchange characteristics of titanate materials,[28−30] the Ag^+ was uniformly distributed in the interlayer of titanate at nanoscale (∼ 1 nm). This provides a platform for the reaction to take place in the nano-space and avoid the aggregation of AgX NPs when reacting with the X^- aqueous solution. Ag NPs were subsequently generated by partial reduction of Ag^+ ions on the surface of AgX upon photo-irradiation, giving rise to SPR effect of the products. The influence of reaction time, pH value, concentration, and type of halogen X^- on the resultant morphologies of AgX, and their photocatalytic decomposition performance towards organic dye molecule were systematically studied.

2. EXPERIMENTAL SECTION

2.1. Preparation of TNHC Films. Titanate nanowired honeycomb (TNHC) films were grown on a titanium foil (0.127 mm thick, Sigma-Aldrich) by a modified hydrothermal method.[27] The titanium foil (5.5 cm × 4.0 cm) was washed by deionized water and then placed perpendicularly to the bottom of a 125 mL Teflon-lined stainless steel autoclave (Parr Instrument). The autoclave was filled with 75 mL of 1.0 M aqueous NaOH solution and kept inside an oven at 220 °C for 6 h. After the hydrothermal reaction, the titanium foil was taken out of the autoclave and immersed in low surface tension ethanol to prevent detachment of the thin film from the foil. Subsequently, hydrogen ion exchange was conducted in 50 mL of 0.10 M HNO_3 solution for 2 h. The samples were then rinsed with deionized water and finally dried at 70 °C. This process was repeated one more time to ensure complete ion exchange leading to complete formation of hydrogen titanate (H-TNHC).

2.2. Preparation of Ag/AgX/TNHC Thin Film by Rapid Injection Method. AgX/TNHC thin films were prepared by a rapid injection method. In a typical procedure, the H-TNHC thin film (1.5 cm × 2.0 cm) was put in 10 mL of 0.10 M $AgNO_3$ aqueous solution at room temperature for 1 h with magnetic stirring (400 rpm), followed by rinsing with ethanol and drying in oven at 70 °C. The obtained silver titanate (Ag-TNHC) film was then placed in a glass beaker where several drops of ethanol were added to wet its surface. Desired reagent HX solutions were injected on the top of the sample. The volume of solution should be enough to cover the thin film surface. After the reaction, the film was removed and rinsed with ethanol or deionized water to remove the reactant solutions. Thereafter, it was dried in a drying cabinet before characterization. Without specific mention, the reaction time to form such AgX/TNHC is 60 s in this work. In the study of the effect of solution pH on the formation of AgX NPs, the pH of the solution was adjusted by adding concentrated NaOH or HNO_3 solution into neutral NaX solution (0.1 M) to ensure the same concentration of X^- ions. Following the formation of AgX/TNHC, the film was irradiated using solar simulator 300 W Xe lamp (HAL-320, Asahi Spectra Co., Ltd.) at an intensity of ca.100 mW/cm^2 for 30 min to yield Ag/AgX/TNHC thin films.

2.3. Sample Characterization. The morphology of the as-synthesized TNHC and AgX/TNHC thin films after reaction were investigated by a field emission scanning electronic microscope (FESEM, JEOL JSM-7600F). A transmission electron microscope (TEM, JEOL JEM-2100F) operating at 200 kV was used to characterize the detailed nanostructures. Energy dispersive X-ray analysis (EDX) was carried out in conjunction with the TEM and FESEM studies. A Bruker D8 Powder X-ray diffractometer (XRD) with a Cu K_α radiation was used for phase identification. UV−visible diffuse reflectance spectra were recorded on a UV-2501 spectrophotometer. The Excalibur Series Fourier transform infrared (FTIR) spectrometer was used to probe the bond types of the samples, and the FTIR absorbance spectra were obtained with 32 scans per sample over the range of 4000−400 cm^{-1}. Photoluminescence (PL) spectrum of the samples was measured using a fluorescence photospectrometer (Varian Cary Eclipse, Australia) at room temperature. All samples were excited at wavelength of 360 nm to measure the emission spectrum.

2.4. Photocatalytic Degradation of Organic Dye. Methyl orange (MO) was chosen as the target compound for the photocatalytic degradation experiments. The batch experiments were conducted in a beaker with Ag/AgX/TNHC thin films (3.0 cm × 2.0 cm) and aqueous solution of MO (5 mg/L, 20 mL) with 400 rpm

dx.doi.org/10.1021/am2015102 | ACS Appl. Mater. Interfaces 2012, 4, 438−446

stirring throughout the test at room temperature. The light-irradiation was performed using a solar simulator 300 W Xe lamp (HAL-320, Asahi Spectra Co., Ltd.) with a super cold filter (YSC0750) to provide visible-light irradiation from 400 to 700 nm. The light intensity was around 95 mW/cm^2. MO concentration at different time intervals was determined quantitatively by the absorption peak generated under a Perkin-Elmer UV−Vis−NIR Lambda 900 spectrophotometer.

3. RESULTS AND DISCUSSION

3.1. Scheme and Characterization of the As-Prepared AgX/TNHC Thin Film Samples. The schematic illustration of the synthesis process for AgX/TNHC heterostructure is shown in Scheme 1. Firstly, sodium TNHC (Na-TNHC, see Figure S1a in the Supporting Information) is formed after the hydrothermal treatment, and then the sample is immersed in HNO_3 solution for hydrogen ion exchange (see Figure S1b in the Supporting Information and Scheme 1a). Secondly, the obtained hydrogen TNHC (H-TNHC) goes through silver ion exchange using $AgNO_3$ solution at room temperature (see Figure S1c in the Supporting Information and Scheme 1b). Thus, Ag^+ ions are uniformly distributed into the nano-scale interlayer of the titanate materials. Finally, silver TNHC (Ag-TNHC) reacts with HX solutions, forming different types of AgX NPs on the TNHC surface (see Figure S1d−f in the Supporting Information and Scheme 1c). The quantitative EDX spectra in Figure S1 in the Supporting Information confirm the elemental composition change during the different processing stages. Typical FESEM and TEM images of the H-TNHC are shown in Figure 1. The as-prepared titanate thin

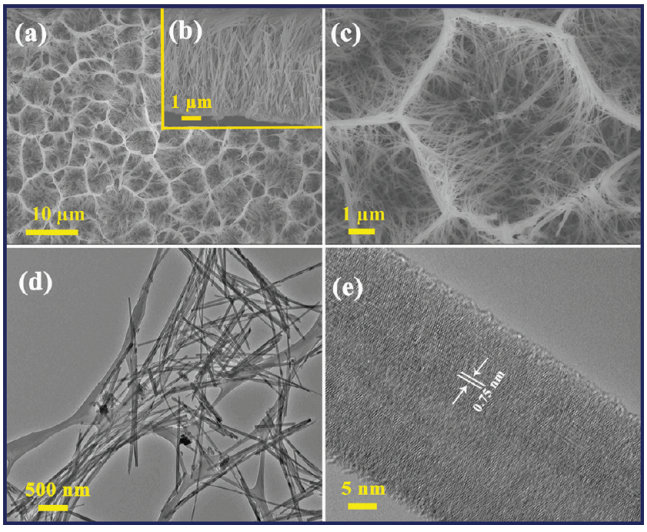

Figure 1. FESEM images of H-TNHC samples taken at (a) low magnification from top view, (b) high magnification from cross-section, and (c) high magnification from top view. TEM images of H-TNHC samples taken at (d) low and (e) high magnifications.

film resembles porous honeycomb structure. Each honeycomb consists of 3−6 sided walls, inside which intertwined titanate nanowires as long as 4.5 ± 1.4 μm are observed (Figure 1a, c). The cross-sectional image (Figure 1b) shows that the H-TNHC network film is perpendicularly grown on the Ti foil, and the thickness of the film is around 5.0 μm. The diameter of a single nanowire is around 45 ± 4 nm (Figure 1d), and the interlayer distance of layered H-TNHC is ca. 0.75 nm from the high-resolution TEM (Figure 1e), which corresponds to the interlayer distance of H-TNHC.

After the reaction between Ag-TNHC and the HX solution, AgX NPs were grown in situ on the TNHC surface. To optimize the experimental parameters, we studied the effect of reaction time, reagent solution concentration, halogen ion species, and pH values on the morphology (size and density) of AgX NPs. To study the influence of reaction time on the AgX particle morphology evolution, the reactions were taken at various time intervals. Figure 2 shows the FESEM images of the

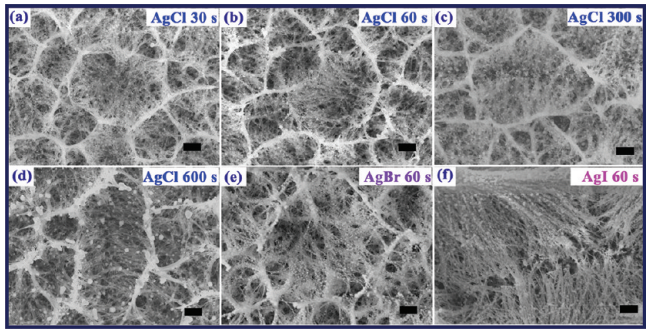

Figure 2. FESEM images of AgCl on TNHC thin film when Ag-TNHC reacted with HCl solution (0.10 M) with durations of (a) 30, (b) 60, (c) 300, and (d) 600 s. (e, f) AgBr and AgI on TNHC thin film when Ag-TNHC reacted with HBr and HI solution (0.10 M) with durations of 60 s, respectively. Scale bar: 1.0 μm.

morphology changes of AgCl NPs under different reaction durations. Meanwhile, the morphology evolution of AgBr and AgI system are shown in Figures S2 and S3 in the Supporting Information, respectively. Before the start of the reaction, the morphology of Ag-TNHC thin film was similar to that of the H-TNHC (0 min, Figure 1a, b) which possesses smooth nanowire surface. After reacting with HCl solution, the dark grey color of the thin film changed to white grey due to the in situ formation of large band gap AgCl NPs on titanate nanowires. From the FESEM images, it is observed that the surface of nanowired-honeycomb thin films was decorated with densely and uniformly distributed AgCl NPs without agglomeration within a short reaction time at room temperature (10 s, see Figure S4 in the Supporting Information). Denser AgCl NPs were formed after reaction for longer time (30−60 s, Figure 2a, b), whereas the particle size had not shown obvious increase. After 300 s of reaction (Figure 2c), some AgCl NPs started to coalesce into large particles, whereas most of the AgCl particles still showed the similar morphology. As the reaction proceeded to 600 s, large-sized NPs (100−650 nm) were observed to form on the honeycomb wall and nanowires (Figure 2d). Therefore, the reaction time is a key factor in controlling the morphology of the AgCl/TNHC thin films. The same phenomenon was observed in the formation process of the AgBr (see Figure S2 in the Supporting Information and Figure 2e) and AgI systems (see Figure S3 in the Supporting Information and Figure 2f). This study finds that the optimum reaction time is 60 s for the generation of uniform and dense AgX crystals on the honeycomb structures (Figure 2b, e, f), so this reaction time was selected for the following experiments.

The influence of solution pH on the formation of AgCl particles on titanate film was studied under the same Cl^- concentration (0.1 M). It is found that dense and uniform distribution of AgCl particles were obtained at pH 1.0 (Figure 2b) and 3.1 (see Figure S5a in the Supporting Information).

dx.doi.org/10.1021/am2015102 | ACS Appl. Mater. Interfaces 2012, 4, 438−446

When the pH value was increased to 6.5 (see Figure S5b in the Supporting Information), particle size became larger. When pH value was beyond 7 (see Figure S5c, d in the Supporting Information), the density of AgCl particles decreased dramatically. We propose that the pH value changes the surface charge of the titanate thin film, which in turn influence the chemical reaction between the titanate thin film and halogen ions.[31,32] According to the previous works,[33,34] the following reactions 1 and 2 are typically used to represent the naked TiO_2 surface in contact with the aqueous media.

$$Ti - OH_2^+ \leftrightarrow Ti - OH + H^+ \quad (1)$$

$$Ti - OH \leftrightarrow Ti - O^- + H^+ \quad (2)$$

Because the titanate materials possess the similar TiO_6 octahedron structure with TiO_2,[29,30,35] their surface reaction is believed to be similar. Therefore, the positive surface charge of titanate film at lower pH value (pH <5) is due to the presence of $TiOH_2^+$ groups,[31,32] which aids the chemical formation of AgCl by prevailing electrostatic attraction between positively charged titanate surface and negatively charged Cl^- ions, and results in the formation of denser AgCl particles. At higher pH value (pH >5) and alkaline conditions, the AgCl nanoparticles are sparse and smaller due to the effect that the emerging $Ti-O^-$ groups with negative surface charges generate repulsive interactions with Cl^- ions. To prove this hypothesis, neutral NaCl, KBr and KI solutions (0.1 M, pH 7.0) were rapidly injected onto the surface of Ag-TNHC thin film to investigate the morphologies of the AgX NPs. As shown in Figure S6 in the Supporting Information, by using neutral reagent solutions, undesirable morphology of silver halide particles were produced compared to the ones obtained by acid HX solution injection (Figure 2b, e, f) because the particles formed were larger and loosely distributed. The resulting morphologies obtained provide additional evidence to support the effect of pH discussed above that electrostatic attraction between the titanate surface and X^- ions can assist the formation of dense and uniform AgX NPs.

Figure 3 presents a series of FESEM images taken from Ag-TNHC samples reacted with different concentrations of Cl^- solutions under acidic conditions. The formations of AgCl NPs across the honeycomb structure of titanate film were successfully achieved for all varying concentrations of HCl solution studied. It was observed that the AgCl particle size synthesized on film was larger (> 150 nm) when low concentration of HCl was used (0.001 M, Figure 3a), which is probably caused by a lower nucleation rate of the AgCl crystals under the low concentration (the total amount of the AgCl crystals, on the other hand, is the same for all samples). Increasing HCl solution concentration (0.01–0.025 M, Figure 3b, c) gave rise to smaller particle size of AgCl nanocrystals (62 ± 25 nm), and the particles were in situ formed along the titanate nanowire direction with higher density and more uniform particle size distribution. When the concentration of HCl solution (0.025–0.05 M, Figure 3c, d) approached 0.05 M, highly densely distributed AgCl particles were obtained with good uniformity. With further increase in HCl solution concentration (0.10 M, Figure 1a), the density of AgCl particles slightly decreased and the particles size was similar. At much higher HCl concentrations (≥1.0 M, Figure 3e, f), the density of the AgCl particle drastically decreased. In particular, under 10 M HCl concentration, there were very few particles observed (Figure 3f), and the thin film might even peeled off

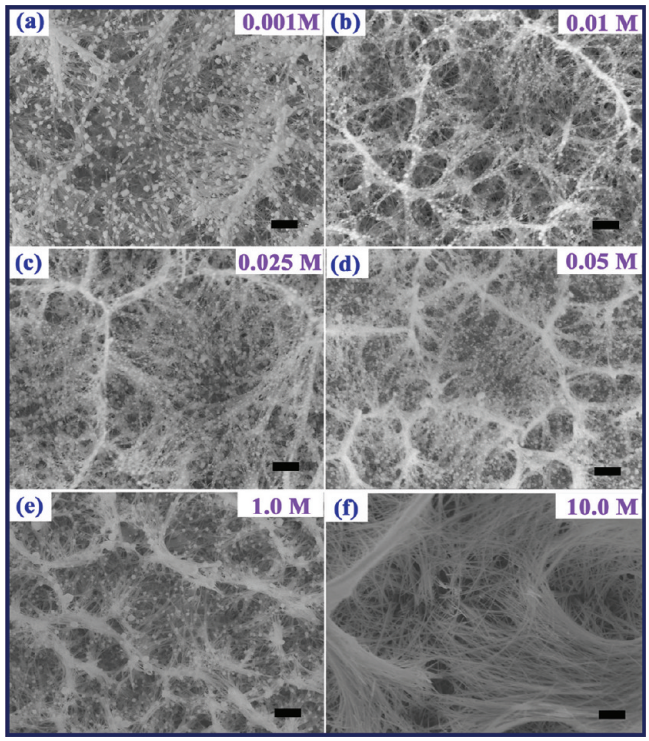

Figure 3. Ag-TNHC reacted with HCl solution with concentrations of (a) 0.001, (b) 0.01, (c) 0.025, (d) 0.05, (e) 1.0, and (f) 10.0 M for a constant reaction time of 60 s. Scale bar: 1.0 μm.

from the substrate. At the same time, many AgCl precipitates were found in the solution, which suggests the reason for the particle disappearance on the surface is due to the corrosive attack to the titanate surface by the high concentration acid. In the AgBr (Figure 2e and Figure S7a,b in the Supporting Information) and AgI systems (Figure 2f and Figure S7c, d in the Supporting Information), it is also found that the tightly clustered NPs were obtained at 0.05 M. This series possess similar trend with that of AgCl formation. For example, as illustrated in Figure 4, the hybridization between the AgI and layered TNHC thin film was confirmed by elemental-mapping analysis with energy-dispersive spectrometry (see Figure S1f in the Supporting Information). Here AgI/TNHC was selected for the elemental-mapping study because of its stability over electron beam irradiation, which can better demonstrate the real distribution of AgX on the thin film. Low-magnification FESEM image of the AgI/TNHC hybrid thin film obtained by injecting 0.05 M HI solution onto TNHC thin film is shown in Figure 4a. The inset image in Figure 4a shows that the AgI NPs were uniformly distributed on titanate nanowires at nanoscale although some NPs tended to aggregate under the electron beam during observation. Figure 4b–d shows the elemental mapping corresponding to oxygen (Figure 4b), silver (Figure 4c), and iodine (Figure 4d). Oxygen, silver and iodine elements were all homogeneously distributed over the entire as-prepared AgI/TNHC hybrids, providing strong evidence for the formation of densely distributed AgI NPs on the layered titanate nanowire structures. For this sample, the molar concentration of AgI and TNHC was about 26 and 74%. With the same approach, the molar concentrations of the AgCl and AgBr were estimated to be 22 and 24%, respectively. According to the above experimental results, we can easily fabricate the densely distributed silver halides (AgX) NPs on

dx.doi.org/10.1021/am2015102 | ACS Appl. Mater. Interfaces 2012, 4, 438–446

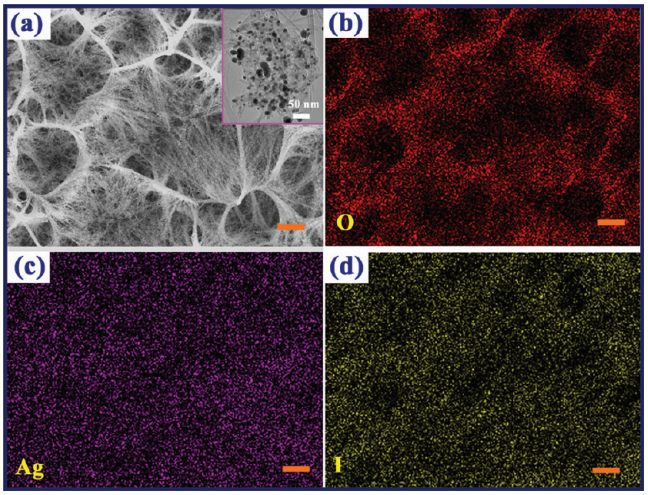

Figure 4. EDX compositional mapping analysis for nano-hybrid AgI/TNHC samples prepared by rapid injection method. (a) SEM images of the AgI/TNHC sample used for EDX analysis, (b) O element mapping, (c) Ag element mapping, and (d) I element mapping. The inset image in (a) is the TEM image of the AgI/TNHC thin film after being peeled off from the substrate via ultrasonic treatment. Scale bar: 2.0 μm.

titanate honeycomb structures via rapidly injecting HX solution (0.05 M) onto Ag-TNHC thin film surface, which are used for the following characterization and photocatalytic performance test.

The XRD result is provided in Figure 5 to understand the crystal structures of silver halides on titanate thin films. The

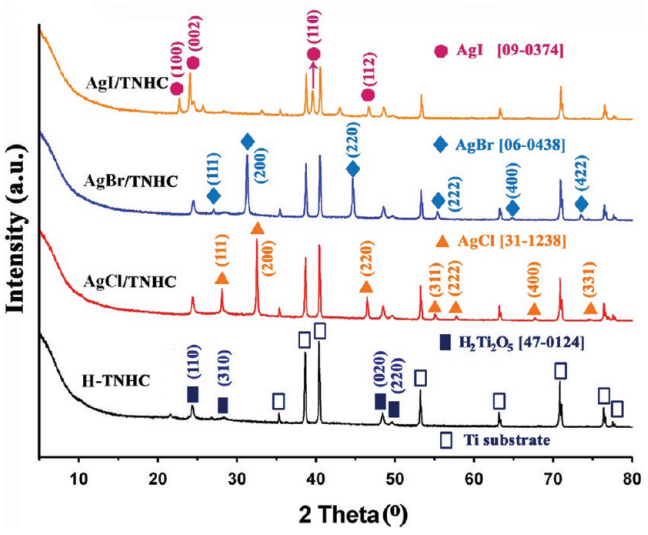

Figure 5. XRD patterns of the as-prepared H-TNHC, AgCl/TNHC, AgBr/TNHC, and AgI/TNHC thin film samples on titanium foils. The AgX/TNHC samples were prepared from Ag-TNHC by rapid injection method with HX solutions (0.05 M).

diffraction pattern of the H-TNHC after hydrothermal synthesis followed by the nitric acid hydrogen ion exchange indicates the formation of orthorhombic $H_2Ti_2O_5 \cdot H_2O$ (JCPDS No. 47-0124) layered crystal structure, which consists of edge sharing TiO_6 octahedral sheet.[36] The peaks at 24.3° (d = 0.366 nm), 28.4° (d = 0.314 nm), 48.5° (d = 0.188 nm), and 49.6° (d = 0.183 nm) correspond to the (110), (310), (020), and (220) planes of the orthorhombic titanate. In the second step, the AgX NPs were introduced to the TNHC thin films by rapid injection method. When the Ag-TNHC reacted with the HCl solution, the AgCl crystals formed instantly. The peaks at 2θ = 28.0° (d = 0.319 nm), 32.5° (d = 0.275 nm), 46.5° (d = 0.195 nm), 55.1° (d = 0.166 nm), 57.7° (d = 0.160 nm), 67.5° (d = 0.138 nm) and 74.5° (d = 0.127 nm) correspond to the (111), (200), (220), (311), (222), (400), and (331) planes of the cubic phase of AgCl with a lattice constant a = 0.555 nm (JCPDS file: 31-1238). Similarly, the face-centered cubic AgBr (JCPDS file: 06-0438) with a lattice constant a = 5.775 nm and hexagonal β-AgI (JCPDS file: 09-0374) nanocrystals were also successfully introduced onto the surface of titanate thin film, as confirmed by the XRD patterns in Figure 5.

The UV–vis absorption spectra of the as-prepared samples are shown in Figure 6a. The strong absorption below a

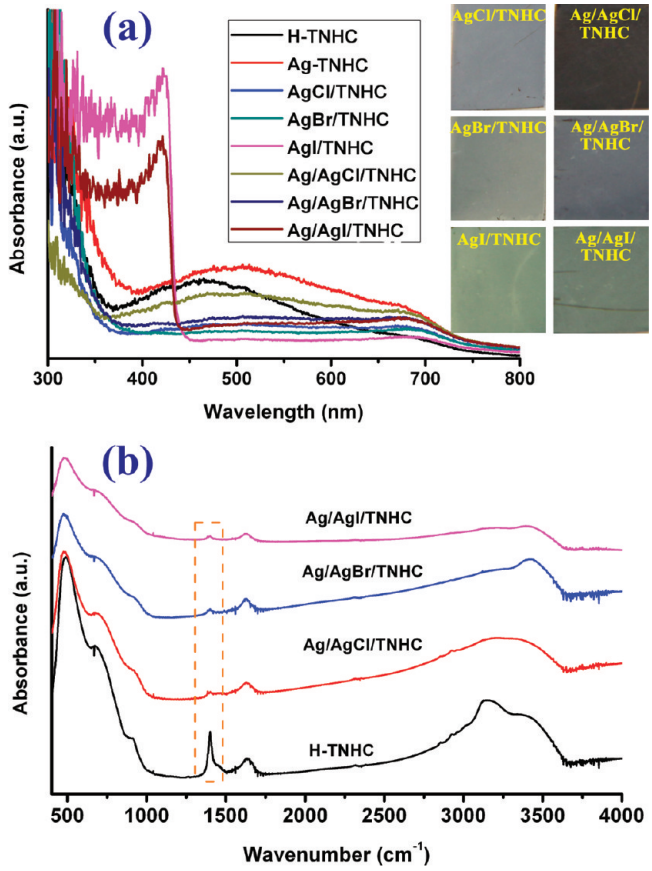

Figure 6. (a) UV–vis absorption spectra of the as-prepared samples of H-TNHC, AgX/TNHC, and Ag/AgX/TNHC samples. (b) FTIR spectra of H-TNHC and Ag/AgX/TNHC samples. The Ag/AgX/TNHC samples were obtained by light illumination of the AgX/TNHC samples, respectively, for 30 min. The inset images in (a) on the right are their corresponding digital photos.

wavelength of 400 nm is associated with the optical band gap of titanate materials, which is the characteristic of titanium oxide-based materials. The absorption spectra were slightly red-shifted when the H-TNHC sample is exchanged with Ag^+ ions (Ag-TNHC). In addition, the H- and Ag-TNHC samples showed a strong visible light absorption ranging from 400 nm to 700 nm (peaked around 450–550 nm), which may be due to the light trapping effect in this unique nanowired-honeycomb structure.[27] When the Ag-TNHC had reacted with HX, AgX

dx.doi.org/10.1021/am2015102 | ACS Appl. Mater. Interfaces 2012, 4, 438–446

NPs formed on the TNHC surface, and the color changed from dark grey to light grey, pale yellow and yellow colors for the AgCl, AgBr and AgI respectively, as shown in the digital photos in the inset of Figure 6a. At the same time, the absorption peak of Ag-TNHC in the visible light region disappeared, which are due to the coverage of surface by different band gap AgX particles. AgCl and AgBr were reported to have a direct band gap of 5.15 eV (indirect band gap 3.25 eV) and 4.25 eV (indirect band gap 2.6 eV) respectively while AgI has a lower direct band gap of 2.8 eV.[37] Thus, the AgI/TNHC sample showed a stronger visible light absorption (380−440 nm) compared with AgCl/TNHC and AgBr/TNHC. According to previous work,[9] the Ag NPs will be partially reduced from the AgX samples to form the surface plasmon Ag/AgX photocatalyst. After Xe lamp illumination for 30 min, the Ag/AgCl/TNHC sample showed a broad plasmonic resonance absorption peak around 500 nm accompanied by a color change from white grey to brown (inset photo in Figure 6a), which indicates the formation of Ag NPs by photoreduction of AgCl. Similarly, the Ag/AgBr/TNHC sample also showed surface plasmon absorption spectrum of Ag NPs (400−700 nm, grey color) but with a lower intensity. Since the AgI samples is more stable under light illumination,[22] the Ag/AgI/TNHC sample exhibited only a weak broad absorption band ranging from 450 to 600 nm (grey yellow color, inset photo in Figure 6a) compared with AgI/TNHC sample, which is consistent with the previously reported result.[8] In addition, the FTIR spectra in Figure 6b are provided to identify the changes of chemical bonding state before and after loading of Ag/AgX nanoparticles on the H-TNHC thin films. It is observed that the Ti−O stretching vibrations, O−H deformation and stretching vibrations came from pure H-TNHC are present at 400−1000, 1625, and 3420 cm^{-1} respectively. Because of the strong interaction between Ti ion and OH groups, a shoulder at 3169 cm^{-1} from Ti−OH bonds is observed, which is in accordance with reported literature.[38,39] Moreover, the spectrum of H-TNHC displays an unknown band at 1398 cm^{-1} (Figure 6b), which could be assigned to the presence of unidentate carbonate groups (C−O).[38] Because the titanate materials have some Ti−O dangling bonds due to the proton vacancy between the TiO_6 interlayers,[40] it can be attached to the O−H, C−O and N−H bonds and so on. After the hybridization with Ag/AgX nanoparticles, intensities of the carbonate bonds are much weaker. This is due to the reduced Ti−O dangling bonds after the loading of Ag/AgX nanoparticles on the H-TNHC surface.

3.2. Photocatalytic Activity of the Ag/AgX/TNHC Thin Film Photocatalysts under Visible Light. To investigate the photocatalytic performance of the optimized Ag/AgX/TNHC samples under simulated visible-light illumination, we tested MO as a target organic compound. For comparison, photocatalytic performance of the H-TNHC was also investigated under the same degradation conditions. As shown in Figure 7a, the Ag/AgX/TNHC composite films exhibited photocatalytic activity for the decomposition of MO under visible light region while H-TNHC itself showed limited or no photocatalytic activity. It was noticed that the Ag/AgCl/TNHC thin film exhibited higher efficiency than the Ag/AgBr/TNHC and Ag/AgI/TNHC. It could completely decompose MO after 160 min irradiation. Furthermore, the cycling performance of Ag/AgCl/THNC was evaluated and shown in Figure 7b by means of performing the MO degradation reaction repeatedly for three times. Interestingly, the samples still show a good photocatalytic activity after recycled usage, and the decrease of the photocatalytic performance is caused by the loss of the catalysts during recycling.[15,27] This provides an evidence that the Ag/AgCl/TNHC sample could be a stable, visible-light photocatalyst.

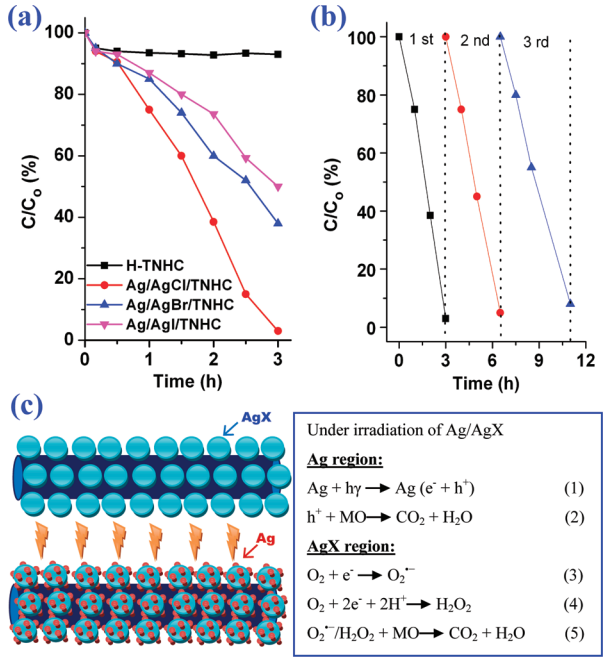

Figure 7. (a) Comparison of photocatalytic activity of different silver/silver halides/titanate films under visible light illumination. C_o (5 ppm) and C are the initial concentration and the concentration of MO after visible-light photodegradation for different time intervals, respectively. (b) Cycling degradation curves for Ag/AgCl/TNHC sample. (c) Schematic illustration of the formation of Ag NPs on AgX surface (left), and the proposed formation of the reactive radicals for the degradation of MO (right).

The current photocatalytic performance of silver halide system appears to lead to different conclusion from Hamal's work.[41] They found that AgI/SiO_2 has higher photoactivity than AgBr/SiO_2 and AgCl/SiO_2. This discrepancy is due to different preparation method and the corresponding material system. We have introduced Ag clusters on the AgX nanoparticle surface making use of the plasmonic effect, which will significantly improve the visible-light photocatalytic activity[15] while Hamal's work depends on the visible light activity of the AgX only. The enhanced visible light absorption due to the SPR effect of Ag NPs on AgCl crystals contributed to the excellent performance of Ag/AgCl/TNHC compared to the Ag/AgBr/TNHC, which had a weaker absorption of visible light (Figure 6). Although the Ag/AgI/TNHC sample showed higher visible light absorption in the wavelength range from 380 nm to 450 nm, the sample showed the lowest photodegradation rate. We suspect that the different photodegradation rate of silver/silver halides might be due to the difference in band gaps and band edge positions, so the charge-separation mechanisms of the silver halides may differ. The proposed formation process, degradation mechanism, energy bands, charge separation of the Ag/AgX photocatalyst are shown in Figures 7c and 8. The energy band diagram and the conduction/valence band position are calculated and summarized in Figure 8 on the basis of the previous work.[37,42−44] After light illumination, some Ag NPs will form due to the partial

dx.doi.org/10.1021/am2015102 | ACS Appl. Mater. Interfaces 2012, 4, 438−446

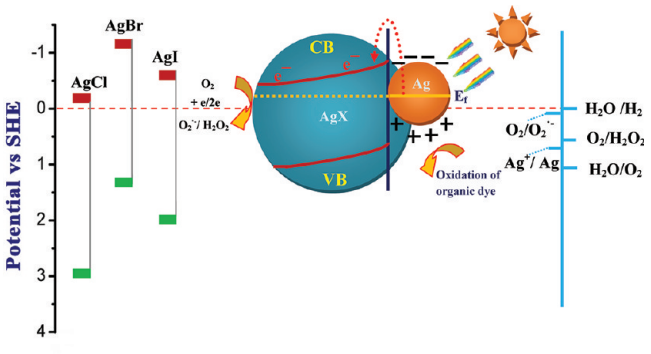

Figure 8. Schematic diagrams showing the self-stabilizing process of the Ag/AgX photocatalyst under visible-light irradiation. Left, position of energy bands of various semiconductors (AgCl, AgBr, and AgI); right, schematic drawing of the possible photocatalytic induction process and charge separation in a visible-light-irradiated Ag/AgX/TNHC system.

reduction of Ag^+ in the AgX samples and generate the surface plasmon Ag/AgX photocatalyst due to the more positive reduction potential of Ag^+/Ag (+0.79 V vs standard hydrogen electrode, SHE). It was reported that the content of Ag^0 is 3−5 % (mol) on AgCl and AgBr,[4,45,46] and the value is almost unchanged upon repeated experiments or long-term use,[16,24,25] which indicates that Ag/AgCl or Ag/AgBr photocatalyst is stable under light illumination. In contrast, most Ag/AgI reported in literatures was prepared via photoreduction of $AgNO_3$ aqueous solution in AgI dispersion due to the high stability of AgI.[8,9] This unique silver/silver halides have special electron-hole separation mechanism different from the traditional metal-semiconductor Schottky barrier that hinders electrons transfer from the metal to the semiconductor. On the basis of work by Hu's group,[8,12] the photogenerated SPR electrons from Ag NPs can transfer to the conduction band (CB) of silver halides (Figure 8), which is beneficial to the stabilization of AgX. The holes escaped from recombination possess a strong oxidation power, which can directly degrade the organic compounds (equation 2 in Figure 7c). Huang's group proposed that the holes can transfer to the AgX surface resulting in the oxidation of X^- ions to X^0 atoms ($h^+ + X^- \rightarrow X^0$).[7,9,22] As X^0 atoms are reactive radical species, they should be able to oxidize MO dye and hence be reduced to X^- ions again.

Considering a more negative potential of the conduction band level of AgX (left of Figure 8) compared with the single electron reduction of oxygen (equation 3 in Figure 7c, +0.13 V vs. SHE) and the multielectron reduction of oxygen (equation 4 in Figure 7c, +0.68 V vs SHE), it is expected that the SPR induced electrons can be trapped by O_2 in the solution to form superoxide ions ($O_2^{\bullet-}$) and reactive hydrogen peroxide species (H_2O_2), which have been proven by early experimental results.[7,8] Therefore, the $O_2^{\bullet-}$, H_2O_2 radicals and holes contribute to the destruction of organic dye via the chemical reaction of equations 2 and 5 in Figure 7c. Because the SPR electrons transfer to the CB of AgX, the electron and hole are efficiently separated. This contributes to the self-stabilizing of the Ag/AgX photocatalyst and the high degradation rate of organic dye.

It is reported that degradation rate of organic dye by Ag/AgX photocatalyst is several times higher than that of N-doped TiO_2 samples.[7] Therefore, the higher photocatalytic activity of Ag/AgCl/TNHC and Ag/AgBr/TNHC is attributed to the efficient electron-hole separation from SPR Ag NPs. Since AgI samples are stable and active (band gap 2.8 eV) under the light illumination, the photocatalytic activity of Ag/AgI/TNHC is mainly contributed from the AgI semiconductor itself, which has higher electron-hole recombination rate and hence lower activity. In order to further clarify this point, photoluminescence (PL) emission spectra of the H-TNHC, Ag/AgCl/TNHC, Ag/AgBr/TNHC, Ag/AgI/TNHC excited at 360 nm are shown in Figure 9. The near-band-edge emission

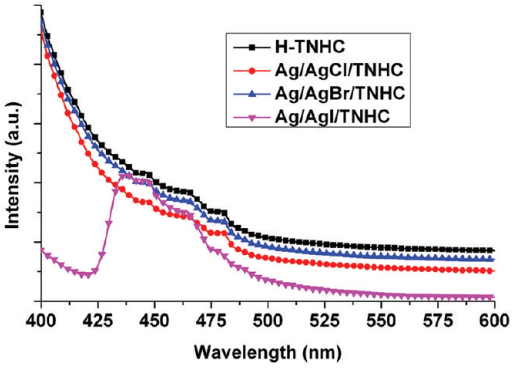

Figure 9. Photoluminescence spectra of H-TNHC and Ag/AgX/TNHC samples with excitation wavelength of 360 nm.

from H-TNHC samples is observed, and several PL peaks above 400 nm arise from the recombination of electrons and holes trapped at various exciton traps such as crystalline defects and impurities. Also, Ag/AgCl/TNHC and Ag/AgBr/TNHC show similar spectra without any new peaks. The intensity is slightly lower than the one of H-TNHC, indicating more efficient electron-hole separation of these two samples. Interestingly, the Ag/AgI/TNHC shows a different PL phenomenon: the near-band-edge emission from H-TNHC is significantly suppressed via the loading Ag/AgI nanoparticles, which indicates that the photoexcited electrons at the conduction band of H-titanate have transferred to that of AgI material. However, we observe a new and strong PL peak around 437 nm (2.84 eV), which has a photon energy equal to that of the band gap of AgI (2.8 eV). This indicates the photoexcited electron at the conduction band edge recombine directly with holes at the valence band edge. Therefore, the different charge carrier separation efficiency of the Ag/AgX/TNHC system could be the reason for the difference in the reported degradation performance.

From the point of view of energy conservation, sunlight is the most attractive candidate to supply energy for the operation of photocatalytic performance.[26] The photodegradation performance of our samples has also been carried out under the simulated sunlight and the results are shown in Figure S8 in the Supporting Information. It is found that the as-prepared Ag/AgX/TNHC samples also show good photocatalytic activity under the simulated sunlight condition while the pure H-TNHC is inactive under the same condition. The increase of the absorption of MO concentration for the H-TNHC samples is due to the evaporation of water under the simulated solar light exposure. As expected, the Ag/AgCl/TNHC still possess the best performance, while the activity of Ag/AgI/TNHC exceeds that of Ag/AgBr/TNHC sample. Conceivably, this enhanced performance of the Ag/AgI/TNHC in photodecolorization of MO dye could be ascribed to more photons absorbed by the Ag/AgI/TNHC under the simulated sunlight

dx.doi.org/10.1021/am2015102 | ACS Appl. Mater. Interfaces 2012, 4, 438−446

compared with visible light condition (Figure 7a), leading to its higher activity under solar light excitation. This result further confirms that the Ag/AgX/TNHC plasmonic photocatalyst is active under the sunlight condition.

4. CONCLUSIONS

In this work, a new strategy combining ion-exchange and rapid chemical reaction was employed to synthesize large-scale AgX (X = Cl, Br, I) nanoparticles on titanate nanowired honeycomb network thin films. The uniformity and density of the AgX NPs depend on the reaction time, pH value, and concentration of the HX solutions reacting with Ag-TNHC thin film. The densely distributed AgX NPs with high uniformity can be obtained at acid conditions within a short time. After the visible light irradiation, the assembled material consisting of Ag/AgX nanoparticles anchored onto titanate nanowired honeycomb network exhibits good photocatalytic activity for the decomposition of an organic dye MO. Among the silver halides, the Ag/AgCl/TNHC hybrid exhibits the highest photocatalytic activity due to the higher surface plasmon effect of Ag NPs, as well as the efficient electron/hole separation by the metal/semiconductor structure. This synthesis method is a generic approach for the fabrication of Ag/AgX/titanate photocatalysts.

■ ASSOCIATED CONTENT

Ⓢ Supporting Information

The EDX spectra of the silver halides on TNHC thin films; FESEM images of AgBr and AgI on TNHC thin films at different experimental conditions; photocatalytic activity of the H-TNHC and Ag/AgX/TNHC photocatalysts for the photodegradation of MO pollutant under simulated sunlight. This material is available free of charge via the Internet at http://pubs.acs.org.

■ AUTHOR INFORMATION

Corresponding Author

*Tel.: +65 6790 4256, +65 6790 6727. Fax: +65 6790 9081. E-mail: aszchen@ntu.edu.sg (Z.C.); zldong@ntu.edu.sg (Z.L.D.);.

■ ACKNOWLEDGMENTS

The authors thank the Environment and Water Industry Programme Office (EWI) under the National Research Foundation of Singapore (Grant MEWR651/06/160) for the financial support of the work.

■ REFERENCES

(1) Maeda, K.; Teramura, K.; Lu, D. L.; Takata, T.; Saito, N.; Inoue, Y.; Domen, K. *Nature* **2006**, *440*, 295−295.
(2) Yi, Z. G.; Ye, J. H.; Kikugawa, N.; Kako, T.; Ouyang, S. X.; Stuart-Williams, H.; Yang, H.; Cao, J. Y.; Luo, W. J.; Li, Z. S.; Liu, Y.; Withers, R. L. *Nat. Mater.* **2010**, *9*, 559−564.
(3) Chen, X. B.; Shen, S. H.; Guo, L. J.; Mao, S. S. *Chem. Rev.* **2010**, *110*, 6503−6570.
(4) Zhu, M. S.; Chen, P. L.; Liu, M. H. *ACS Nano* **2011**, *5*, 4529−4536.
(5) Zhang, J.; Li, S. Z.; Wu, J. S.; Schatz, G. C.; Mirkin, C. A. *Angew. Chem., Int. Ed.* **2009**, *48*, 7787−7791.
(6) Elahifard, M. R.; Rahimnejad, S.; Haghighi, S.; Gholami, M. R. *J. Am. Chem. Soc.* **2007**, *129*, 9552−9553.
(7) Wang, P.; Huang, B. B.; Qin, X. Y.; Zhang, X. Y.; Dai, Y.; Wei, J. Y.; Whangbo, M. H. *Angew. Chem., Int. Ed.* **2008**, *47*, 7931−7933.
(8) Hu, C.; Peng, T. W.; Hu, X. X.; Nie, Y. L.; Zhou, X. F.; Qu, J. H.; He, H. *J. Am. Chem. Soc.* **2010**, *132*, 857−862.
(9) Wang, P.; Huang, B. B.; Zhang, X. Y.; Qin, X. Y.; Jin, H.; Dai, Y.; Wang, Z. Y.; Wei, J. Y.; Zhan, J.; Wang, S. Y.; Wang, J. P.; Whangbo, M. H. *Chem.--Eur. J.* **2009**, *15*, 1821−1824.
(10) Zhai, Y.; Han, L.; Wang, P.; Li, G.; Ren, W.; Liu, L.; Wang, E.; Dong, S. *ACS Nano* **2011**, *5*, 8562−8570.
(11) Hu, C.; Hu, X.; Wang, L.; Qu, J.; Wang, A. *Environ. Sci. Technol.* **2006**, *40*, 7903−7907.
(12) Hu, C.; Lan, Y. Q.; Qu, J. H.; Hu, X. X.; Wang, A. M. *J. Phys. Chem. B* **2006**, *110*, 4066−4072.
(13) Lan, Y. Q.; Hu, C.; Hu, X. X.; Qu, J. H. *Appl. Catal., B* **2007**, *73*, 354−360.
(14) Bi, Y. P.; Ye, J. H. *Chem. Commun.* **2009**, 6551−6553.
(15) Yu, J. G.; Dai, G. P.; Huang, B. B. *J. Phys. Chem. C* **2009**, *113*, 16394−16401.
(16) An, C. H.; Peng, S. N.; Sun, Y. G. *Adv. Mater.* **2010**, *22*, 2570−2574.
(17) Bi, Y. P.; Ye, J. H. *Chem.—Eur. J.* **2010**, *16*, 10327−10331.
(18) Wang, X.; Li, S.; Yu, H.; Yu, J.; Liu, S. *Chem.—Eur. J.* **2011**, *17*, 7777−7780.
(19) Jiang, J.; Zhang, L. *Chem.—Eur. J.* **2011**, *17*, 3710−3717.
(20) Xu, H.; Li, H.; Xia, J.; Yin, S.; Luo, Z.; Liu, L.; Xu, L. *ACS Appl. Mater. Interfaces* **2010**, *3*, 22−29.
(21) Elahifard, M. R.; Rahimnejad, S.; Haghighi, S.; Gholami, M. R. *J. Am. Chem. Soc.* **2007**, *129*, 9552−9553.
(22) Wang, P.; Huang, B. B.; Zhang, Q. Q.; Zhang, X. Y.; Qin, X. Y.; Dai, Y.; Zhan, J.; Yu, J. X.; Liu, H. X.; Lou, Z. Z. *Chem.—Eur. J.* **2010**, *16*, 10042−10047.
(23) Cheng, H.; Huang, B.; Wang, P.; Wang, Z.; Lou, Z.; Wang, J.; Qin, X.; Zhang, X.; Dai, Y. *Chem. Commun.* **2011**, *47*, 7054−7056.
(24) Sun, Y. G. *J. Phys. Chem. C* **2010**, *114*, 2127−2133.
(25) Zhang, H.; Fan, X. F.; Quan, X.; Chen, S.; Yu, H. T. *Environ. Sci. Technol.* **2011**, *45*, 5731−5736.
(26) Zhu, M.; Chen, P.; Liu, M. *J. Mater. Chem.* **2011**, *21*, 16413−16419.
(27) Tang, Y. X.; Subramaniam, V. P.; Lau, T. H.; Lai, Y. K.; Gong, D. G.; Kanhere, P. D.; Cheng, Y. H.; Chen, Z.; Dong, Z. L. *Appl. Catal., B* **2011**, *106*, 577−585.
(28) Kasuga, T.; Hiramatsu, M.; Hoson, A.; Sekino, T.; Niihara, K. *Adv. Mater.* **1999**, *11*, 1307−1311.
(29) Sun, X. M.; Li, Y. D. *Chem.—Eur. J.* **2003**, *9*, 2229−2238.
(30) Yang, D. J.; Zheng, Z. F.; Zhu, H. Y.; Liu, H. W.; Gao, X. P. *Adv. Mater.* **2008**, *20*, 2777−2781.
(31) Lai, Y. K.; Chen, Y. C.; Tang, Y. X.; Gong, D. G.; Chen, Z.; Lin, C. J. *Electrochem. Commun.* **2009**, *11*, 2268−2271.
(32) Tang, Y. X.; Gong, D. G.; Lai, Y. K.; Shen, Y. Q.; Zhang, Y. Y.; Huang, Y. Z.; Tao, J.; Lin, C. J.; Dong, Z. L.; Chen, Z. *J. Mater. Chem.* **2010**, *20*, 10169−10178.
(33) Vohra, M. S.; Kim, S.; Choi, W. *J. Photochem. Photobiol., A* **2003**, *160*, 55−60.
(34) Park, H.; Choi, W. *J. Phys. Chem. B* **2005**, *109*, 11667−11674.
(35) Cheng, Y. H.; Huang, Y. Z.; Kanhere, P. D.; Subramaniam, V. P.; Gong, D. G.; Zhang, S.; Highfield, J.; Schreyer, M. K.; Chen, Z. *Chem.—Eur. J.* **2011**, *17*, 2575−2578.
(36) Gao, T.; Fjellvag, H.; Norby, P. *Inorg. Chem.* **2009**, *48*, 1423−1430.
(37) Glaus, S.; Calzaferri, G. *Photochem. Photobiol. Sci.* **2003**, *2*, 398−401.
(38) Peng, C.-W.; Richard-Plouet, M.; Ke, T.-Y.; Lee, C.-Y.; Chiu, H.-T.; Marhic, C.; Puzenat, E.; Lemoigno, F.; Brohan, L. *Chem. Mater.* **2008**, *20*, 7228−7236.
(39) Lim, Y. W. L.; Tang, Y. X.; Cheng, Y. H.; Chen, Z. *Nanoscale* **2010**, *2*, 2751−2757.
(40) Zhou, W.; Liu, H.; Boughton, R. I.; Du, G.; Lin, J.; Wang, J.; Liu, D. *J. Mater. Chem.* **2010**, *20*, 5993−6008.
(41) Hamal Dambar, B.; Klabunde Kenneth, J. *Nanoscale Materials in Chemistry: Environmental Applications*; American Chemical Society: Washington, D.C., 2010; Vol. *1045*; pp 191−205.
(42) Zhang, L.; Wong, K.-H.; Chen, Z.; Yu, J. C.; Zhao, J.; Hu, C.; Chan, C.-Y.; Wong, P.-K. *Appl. Catal., A* **2009**, *363*, 221−229.

(43) Wang, X.; Li, S.; Ma, Y.; Yu, H.; Yu, J. *J. Phys. Chem. C* **2011**, *115*, 14648−14655.
(44) Cheng, H.; Huang, B.; Dai, Y.; Qin, X.; Zhang, X. *Langmuir* **2010**, *26*, 6618−6624.
(45) Wang, P.; Huang, B. B.; Lou, Z. Z.; Zhang, X. Y.; Qin, X. Y.; Dai, Y.; Zheng, Z. K.; Wang, X. N. *Chem.—Eur. J.* **2010**, *16*, 538−544.
(46) Wang, P.; Huang, B. B.; Zhang, X. Y.; Qin, X. Y.; Dai, Y.; Wang, Z. Y.; Lou, Z. Z. *Chemcatchem* **2011**, *3*, 360−364.